BNL-113175-2016-JA

Mechanism of Photocatalytic Reduction of CO2 by Re(bpy)(CO)(3)Cl from Differences in Carbon Isotope Discrimination

Taylor Schneider, Mehmed Z. Ertem, James T. Muckerman, Alfredo M. Angeles-Boza

Submitted to ACS Catalysis

August 2016

Chemistry Department

Brookhaven National Laboratory

U.S. Department of Energy
USDOE Office of Science (SC),
Basic Energy Sciences (BES) (SC-22)

DISCLAIMER

Mechanism of Photocatalytic Reduction of CO_2 by $Re(bpy)(CO)_3Cl$ from Differences in Carbon Isotope Discrimination

Taylor Schneider,[†] Mehmed Z. Ertem,[‡,] James T. Muckerman,[‡] Alfredo M. Angeles-Boza[†,*]*

[†]Department of Chemistry, University of Connecticut, Storrs, Connecticut 06269-3060

[‡]Chemistry Division, Energy & Photon Sciences Directorate, Brookhaven National Laboratory, Bldg. 555A, Upton, New York 11973

KEYWORDS: CO_2 reduction, photocatalysis, homogeneous catalysis, isotope effects, isotopic discrimination.

ABSTRACT: The rhenium complex $Re(bpy)(CO)_3Cl$ (**1**, bpy = 2,2'-bipyridine) catalyzes CO_2 reduction to CO in mixtures containing triethanolamine (TEOA) as a sacrificial reductant. The mechanism of this reaction under photocatalytic conditions remains to be fully characterized. Here, we report the competitive carbon kinetic isotope effects (^{13}C–KIEs) on photocatalytic CO_2 reduction by **1** and analyze the results of experimental measurements by comparing with computed KIEs via density functional theory (DFT) calculations as a means of formulating a chemical mechanism and illustrating the utility of this approach. The ^{13}C-KIEs, $k(^{12}C)/k(^{13}C)$, in acetonitrile (ACN) and dimethylformamide (DMF) were determined to be 1.0718 ± 0.0036 and 1.0685 ± 0.0075, respectively. When $[Ru(bpy)_3]Cl_2$ is added to the reaction mixture in acetonitrile as a photosensitizer, the reduction of CO_2 exhibited a ^{13}C-KIE = 1.0703 ± 0.0043. These values are consistent with the calculated isotope effect of CO_2 binding to the one-electron reduced $[Re^{I}(bpy^{\bullet -})(CO)_3]$ species. The findings reported here provide strong evidence that the reactions in the two different solvents have the same first irreversible step and proceed with similar reactive intermediates upon reduction. Theoretically, we found that the major contribution for the large ^{13}C isotope effects comes from a dominant zero-point energy (ZPE) term. These results lay the groundwork for combined experimental and theoretical approaches for analysis of competitive isotope effects towards understanding CO_2 reduction catalyzed by other complexes.

INTRODUCTION

Catalytic reactions of carbon dioxide reduction have attracted much attention as an important component of artificial photosynthesis and because of concerns over increasing concentrations of this greenhouse gas in the atmosphere.[1] A variety of systems, both homogenous and heterogeneous, have been shown to be active catalysts for CO_2 reduction.[2-18] Despite the advances made in this field, the origins of the catalytic rate enhancement achieved by many of these systems remain to be fully understood.[19-23] This is particularly true when it comes to mechanistic details of the bond forming and bond breaking steps accompanying the reduction of CO_2.

Among the catalysts for CO_2 reduction, $Re(bpy)(CO)_3Cl$ (**1**, bpy = 2,2'-bipyridine) and its derivatives have been recognized as being very active and selective for reduction of CO_2 to CO.[24-29] Photocatalytic reduction of CO_2 to CO in the presence of sacrificial electron donors has been reported for **1**. The mechanism of the photochemical CO_2 reduction has been studied by a number of techniques including UV-visible absorption spectroscopy, infrared spectroscopy, electron spin resonance and mass spectrometry.[19,27,30-37] On the basis of these studies, plausible mechanisms have been proposed.[20,38] The key equations involved in the proposed mechanisms are shown in Eqs 1-6. Upon photoexcitation, the triplet metal-to-ligand charge transfer (^{3}MLCT) state of **1** is produced. In the presence of a sacrificial electron donor such as TEOA, the ^{3}MLCT excited state is reductively quenched.[35] Upon reduction, the Re complex eliminates the chloride ion, which results in an available coordinating site. CO_2 is known to bind to singly reduced rhenium species, for example, the 17-electron species $[Re^0(bpy)(CO)_3]$ or $[Re^I(bpy^{\bullet -})(CO)_3]$ (eq

2).[24] Alternatively, the 18-electron species $[Re^{I}(bpy)(CO)_3]^-$ is also a plausible nucleophile,[24] although deemed to be less likely when TEOA is used as the sacrificial electron donor. After binding, CO_2 is reduced to CO and H_2O with multiple protonation steps.

$$(1)\quad [(bpy)(CO)_3Re^{I}\text{-}Cl] + [red] \underset{k_{-1}}{\overset{k_1}{\rightleftharpoons}} [(bpy)(CO)_3Re^{0}] + [ox] + Cl^-$$

$$(2)\quad [(bpy)(CO)_3Re^{0}] + CO_2 \underset{k_{-2}}{\overset{k_2}{\rightleftharpoons}} [(bpy)(CO)_3Re\text{-}CO_2]$$

$$(3)\quad [(bpy)(CO)_3Re\text{-}CO_2] + [red] \underset{k_{-3}}{\overset{k_3}{\rightleftharpoons}} [(bpy)(CO)_3Re\text{-}CO_2]^- + [ox]$$

$$(4)\quad [(bpy)(CO)_3Re\text{-}CO_2]^- + 2H^+ \underset{k_{-4}}{\overset{k_4}{\rightleftharpoons}} [(bpy)(CO)_3Re^{I}\text{-}CO]^+ + H_2O$$

$$(5)\quad [(bpy)(CO)_3Re^{0}] + [red] \underset{k_{-5}}{\overset{k_5}{\rightleftharpoons}} [(bpy)(CO)_3Re^{-1}]^- + [ox]$$

$$(6)\quad [(bpy)(CO)_3Re^{-1}]^- + CO_2 \underset{k_{-6}}{\overset{k_6}{\rightleftharpoons}} [(bpy)(CO)_3Re\text{-}CO_2]^-$$

In addition, a binuclear pathway involving a rhenium dimer carboxylate intermediate is also proposed based on the work by Fujita and co-workers in which a one-electron-reduced species of a derivative of **1**, $Re^{0}(dmb)(CO)_3$ (dmb = 4,4'-dimethyl-2,2'-bipyridine), is prepared by photocleavage of the Re-Re bond of $[Re(dmb)(CO)_3]_2$.[37,39] Furthermore, rhenium-carbonate (**A**) and -iminoester (**B**) species have been reported to form during the photochemical reduction of CO_2 by **1** (Figure 1).[19] The former forms via the insertion of CO_2 into the TEOA adduct, $[Re(bpy)(CO)_3(TEOA)]^+$, when the solvent is DMF, whereas the latter is the product of the attack of TEOA on the acetonitrile (ACN) ligand in $[Re^{I}(bpy)(CO)_3(ACN)]^+$ when the reaction is performed in ACN .[19] The former species has recently been proposed as the active form of the

catalyst in the photoreduction of CO_2 in the presence of TEOA in DMF. However, the chemical details of this conversion have yet to be clarified.

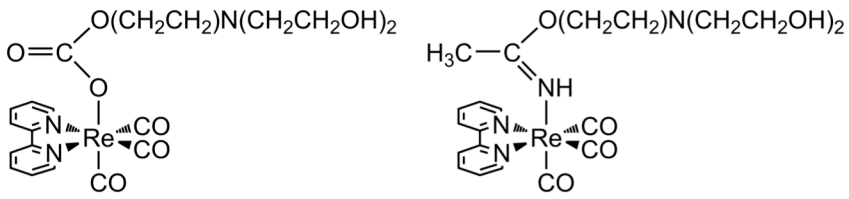

Figure 1. Schematic representation of the carbonate (**A**) and iminoester (**B**) species formed during the photochemical reduction of CO_2 in DMF and ACN, respectively.

Competitive kinetic isotope effects (KIEs) at natural abundance levels have provided direct information about the nature of the transition state in enzymatic and nonenzymatic reactions.[40,41] KIEs arise from changes in the bond orders of the substrate between the ground state and the transition state. For example, determination of oxygen isotope discrimination was used to identify the mechanisms of O-O bond formation of water oxidation reactions catalyzed by iron and ruthenium complexes.[42-44] These studies indicate that competitive KIEs in combination with density functional theory (DFT) calculations can discern between distinct O-O formation pathways such as water nucleophilic attack and the interaction of two oxo moieties. More recently, ^{18}O–KIEs and computational studies were employed to determine that the first irreversible and rate-determining step in the catalytic O_2 evolution cycle of an oxomanganese complex is substrate binding to the catalyst, not the formation of the Mn-oxo/oxyl species as previously assumed.[45] These reports highlight the power of the methodology to study complex inorganic reaction mechanisms containing multiple isotopically sensitive steps.[42,46,47]

In the present work, we combine high precision *natural abundance* competitive ^{13}C–KIEs measurements with computed isotope effects via density functional theory (DFT) calculations to examine the mechanism of photochemical CO_2 reduction by **1.** We further analyze the ^{13}C–KIEs using an established competitive methodology to shed light on the mechanistic details such as the irreversible and rate determining steps associated with photochemical conversion of CO_2 to CO by **1**.

RESULTS

Experimental Kinetic Isotope Effects. The ^{13}C–KIEs for carbon dioxide reduction were measured using an established competitive methodology.[48] The apparatus design and methodology is described in detail in the experimental section. The required equipment can be easily constructed by a professional glassblower. Solutions of TEOA in acetonitrile (ACN) or dimethylformamide (DMF) were saturated with 3% CO_2 in N_2 prior to initiating reactions by adding a fixed volume of the saturated solution to an evacuated flask containing the catalyst. The reaction mixtures were stirred and photoirradiated before collecting the *unreacted* CO_2. A series of cold traps were used to remove impurities (*e.g.,* solvent, CO) prior to the collection of pure CO_2. Pressures of the unreacted CO_2 were determined using a calibrated manometer to determine the extent of the reaction. As previously reported by Hawecker *et al*., no background reaction of CO_2 was detected in the absence of the catalyst. The change in the $^{13}C/^{12}C$ and $^{18}O/^{16}O$ ratios of unreacted starting material at varying fractional conversions was analyzed by isotope ratio mass spectrometry (IRMS) analysis (Figure 2). The degree of fractionation was also determined using the photosensitizer $[Ru(bpy)_3]Cl_2$. $[Ru(bpy)_3]^{2+}$ is an outer sphere electron transfer reagent with a bimolecular self-exchange rate constant approaching the diffusion limit.[49] Equimolar mixtures of $[Ru(dmb)_3]^{2+}$ (dmb = 4,4'-dimethyl-2,2'-bipyridine) and $Re(dmb)(CO)_3Cl$ have larger turnover

numbers (100 after 16 h irradiation) than the catalyst alone (15 under the same conditions) for CO formation.[50] The reason for this acceleration is attributed to the accumulation of additional reducing equivalents that increase the rate of the second electron transfer.[32] When $[Ru(bpy)_3]Cl_2$ was used, the experimental procedure described above was varied by introducing the solutions of TEOA in either ACN or DMF saturated with 3% CO_2 in N_2 into a sealed reaction vessel containing both the catalyst and photosensitizer.

Competitive KIEs were determined fitting the data to the Rayleigh equation (eq 7)

$$\frac{R_f}{R_0} = (1-f)^{\frac{1}{KIE}-1} \qquad (7)$$

where R_f and R_0 are the isotopic ratios ($^{12}C/^{13}C$) in the remaining CO_2 and initial CO_2, respectively, and f is the fraction of unreacted CO_2.[51] The error bars shown in Fig. 2 correspond to the uncertainty associated with the measurement of carbon dioxide samples during calibration of the apparatus. The ^{13}C–KIEs, $k(^{12}C)/k(^{13}C)$, for the photochemical reduction of CO_2 catalyzed by **1** were determined to be 1.0718 ± 0.0036 and 1.0685 ± 0.0075 in ACN and DMF, respectively. In the presence of $[Ru(bpy)_3]Cl_2$, the photochemical reduction of CO_2 exhibited a ^{13}C–KIE = 1.0703 ± 0.0043 (Figure 2).

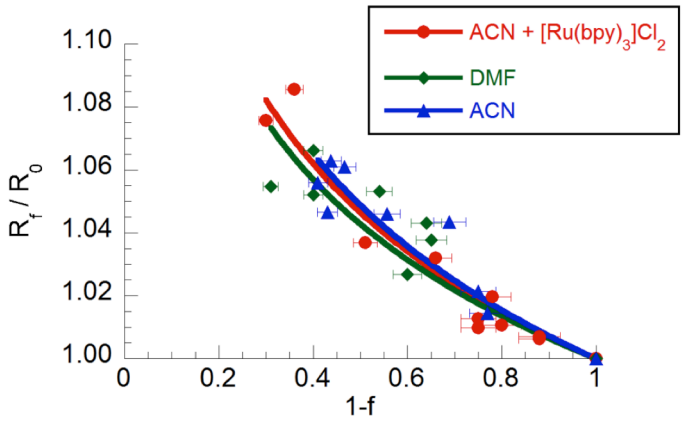

Figure 2. Isotope fractionation of photochemical CO_2 reduction catalyzed by complex **1**. Plot of the theoretical curve of R_f / R_0 vs (1 - f) according to eq 7. All of the data points are shown

The experiments were also expected to determine the ^{18}O–KIEs; however, the oxygen atoms are exchanged under the reaction conditions, not allowing accurate determination of isotope fractionations. When the isotopic composition of samples of CO_2 incubated with catalyst and TEOA in ACN without exposure to light were measured, the $\delta^{13}C$ ranged from −15 ‰ to −14.2 ‰, whereas the $\delta^{18}O$ varied from −22.6 ‰ to −14.6 ‰. This result indicated exchange of the oxygen atoms, large enough to affect the measurements. Less exchange was observed in DMF but it was still too large to obtain reliable ^{18}O–KIE measurements. The exchange of oxygen atoms might be due to the presence of H_2O in the solvent.

Theoretical Investigation of the CO_2 Reduction Mechanism of 1. Density functional theory (DFT) calculations at the M06 level of theory coupled with the SMD continuum solvation method (*see computational methods for details*) were used to examine the reaction mechanism of CO_2 reduction by **1** and to compute the ^{13}C–KIEs associated with the optimized transition state structures. The computed free-energy changes for the proposed CO_2 reduction mechanism in ACN are summarized in Scheme 1 and the results for DMF as the solvent are presented in Scheme S2. The results for the initial activation and reduction steps of the catalyst with chloride (*e.g.*, $[Re^{I}(bpy)(CO)_3Cl]^0$) or solvent molecules (*e.g.*, $[Re^{I}(bpy)(CO)_3(ACN)]^+$ or $[Re^{I}(bpy)(CO)_3(DMF)]^+$) as ligands are reported in the SI and are similar to those previously reported in the literature (Scheme S1). Hence, the initial species in Scheme 1 is the one-electron-reduced, 17-electron $[Re^0(bpy)(CO)_3]$ complex generated via reductive quenching of the excited ^{3}MLCT state of **1** by TEOA. The first step of the proposed mechanism involves binding of CO_2 to $[Re^0(bpy)(CO)_3]$, which proceeds with a free energy of activation ($\Delta G^{\ddagger}$) of 24.6 kcal/mol. This value is higher than the computed activation free energy for the binding of CO_2 to the two-electron-reduced species $[Re^{-I}(bpy)(CO)_3]^-$ ($\Delta G^{\ddagger}$ = 16.1 kcal/mol). This is not unexpected given

the fact that the two-electron-reduced species is a better nucleophile.[24] Indeed, both calculated $\Delta G^{\ddagger}$ values agree well with the activation free-energy barriers estimated from reported pseudo first-order rate constants for $[Re^{I}(bpy)(CO)_3]^-$ and the $[Re^{0}(bpy)(CO)_3]$ species reacting with CO_2. Within the adiabatic limit, the $\Delta G^{\ddagger}$ for the reaction of $[Re^{0}(bpy)(CO)_3S]$ (S = tetrahydrofuran) with CO_2 is *ca*. 22 kcal/mol, whereas that of $[Re^{I}(bpy)(CO)_3]^-$ is 15 kcal/mol.[37,52] After the reaction of the $[Re^{0}(bpy)(CO)_3]$ with CO_2, a second reduction could occur to produce the anionic intermediate $[Re^{I}(CO_2)(bpy)(CO)_3]^-$ with a computed reduction potential of E = −1.26 V vs SCE (Scheme 1). This reduction step is predicted to be facile given the relatively low free-energy requirement compared to initial reduction events (Scheme S1). The metallocarboxylate intermediate, $[Re^{I}(CO_2)(bpy)(CO)_3]^-$, can then undergo protonation in a barrierless, highly exoergic (ΔG = −23.9 kcal/mol with $TEOAH^+$ as the proton source) step to generate $[Re^{I}(CO_2H)(bpy)(CO)_3]$. The following steps involve C−OH bond breakage to form CO by either protonation–reduction or reduction–protonation steps (Scheme 1).[22] The protonation–reduction pathway starts with the breakage of the C−OH bond in $[Re^{I}(CO_2H)(bpy)(CO)_3]$ with $TEOAH^+$ as the proton source (*see computational methods for details*) and the optimized transition state structure features a $\Delta G^{\ddagger}$ of 18.2 kcal/mol. The protonation step is downhill with ΔG = −8.3 kcal/mol, partly due to entropic gain by release of an H_2O molecule, and is followed by a reduction step with an associated potential of E = −1.52 V to generate $[Re^{0}(bpy)(CO)_4]$. On the other hand, the initial step of the reduction–protonation pathway is the reduction of $[Re^{I}(CO_2H)(bpy)(CO)_3]$ to $[Re^{0}(CO_2H)(bpy)(CO)_3]^-$ with E = −1.88 V, followed by concerted protonation and C−OH bond breakage with $\Delta G^{\ddagger}$ = 11.3 kcal/mol. The evolution of CO from the final product of both pathways, $[Re^{0}(bpy)(CO)_4]$, completes the catalytic cycle and regenerates

$[Re^{0}(bpy)(CO)_3]$ or $[Re^{I}(bpy)(CO)_3]^-$ with further reduction. The reduction first pathway has been proposed as the preferred route in electrocatalytic reduction of CO_2 by **1**[22] but given the relatively low activation free energies for protonation in the presence of $TEOAH^+$, it is hard to conclude which path will be preferred in photochemical CO_2 reduction by **1**. However, as will be discussed in the next sections, the contribution to competitive ^{13}C–KIEs is computed to be similar for both pathways.

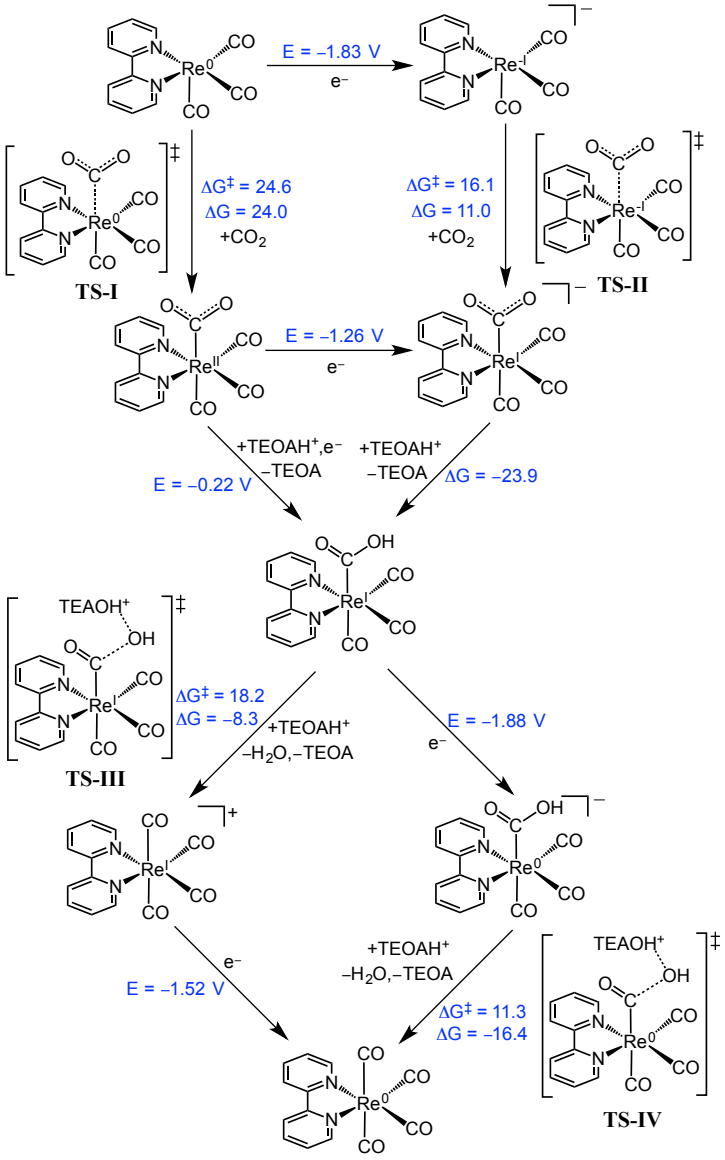

Scheme 1. Reaction mechanism of CO_2 reduction by the precatalyst **1** in ACN obtained at the M06 level of theory. The free-energy changes (ΔG) and activation free energies ($\Delta G^{\ddagger}$) are reported in units of kcal/mol and reduction potentials (E) in units of volts vs SCE.

Equilibrium isotope effects (EIEs) and KIEs were calculated for each reaction step from the computed vibrational frequencies of the optimized structures using the Bigeleisen and Goeppert-Mayer approach, in accord with the Redlich-Teller Product Rule, using the generic isotope equation A + B* → A* + B, where the asterisk designates the site of the heavy isotope, as follows:[53,54]

$$\mathrm{KIE} = ({}^{13}\nu_{\mathrm{RC}})\,(ZPE \times EXC \times VP) \tag{8}$$

$$\mathrm{EIE} = ZPE \times EXC \times MMI \tag{9}$$

$$ZPE = \frac{\left[\prod_{j}^{3N-6} \frac{\exp(h\nu_j^{B*}/(2kT))}{\exp(h\nu_j^{B}/(2kT))}\right]}{\left[\prod_{i}^{3N-6} \frac{\exp(h\nu_i^{A*}/(2kT))}{\exp(h\nu_i^{A}/(2kT))}\right]} \tag{10}$$

$$EXC = \frac{\left[\prod_{j}^{3N-6} \frac{1-\exp\{-(h\nu_j^{B*}/(kT))\}}{1-\exp\{-(h\nu_j^{B}/(kT))\}}\right]}{\left[\prod_{i}^{3N-6} \frac{1-\exp\{-(h\nu_i^{A*}/(kT))\}}{1-\exp\{-(h\nu_i^{A}/(kT))\}}\right]} \tag{11}$$

$$MMI = \frac{\prod_{j}^{3N-6} (\nu_j^{B}/\nu_j^{B*})}{\prod_{i}^{3N-6} (\nu_i^{A}/\nu_i^{A*})} \tag{12}$$

$$VP = \frac{\prod_{j}^{3N-7} (\nu_j^{B}/\nu_j^{B*})}{}$$

(13)

where $^{13}\nu_{RC}$ is the ratio of the imaginary frequencies of the transition states associated with light, ^{12}C, and heavy, ^{13}C, isotopologues, ZPE is zero point energy, EXC is vibrational excitation energy, MMI is mass of moments of inertia and VP is vibrational product. Other terms in equations 10 and 11 include Boltzmann's constant (*k*), Planck's constant (*h*), and temperature (*T*). The ^{13}C–KIEs were computed for both the CO_2 binding and C–OH bond cleavage steps, the results of which are presented in Table 1. The computed intrinsic ^{13}C–KIEs for CO_2 binding by $[Re^{I}(bpy)(CO)_3]^-$ and $[Re^{0}(bpy)(CO)_3]$ are 1.086 and 1.061, respectively, in ACN, and 1.088 and 1.065 in DMF (Table S1). These values are consistent with KIEs reported for binding of small molecules to transition metals as well as ^{13}C–KIEs measurements for **1** of 1.072 and 1.068 in ACN and DMF, respectively. The C–OH cleavage steps in either $[Re^{I}(CO_2H)(bpy)(CO)_3]$ or $[Re^{0}(CO_2H)(bpy)(CO)_3]^-$ result in smaller intrinsic ^{13}C–KIEs of 1.048 (Table 1 and Table S1). The ^{13}C–KIE measurements indicate that the first irreversible step determining the isotope fractionation is the same for photochemical conversion of CO_2 to CO by **1** in ACN and DMF. Based on computed ^{13}C–KIEs, this step is assigned to the binding of CO_2 to the one-electron-reduced $[Re^{0}(bpy)(CO)_3]$ species. CO_2 binding to the further reduced $[Re^{I}(bpy)(CO)_3]^-$ species is less likely to be the first irreversible step for two reasons: (i) the computed ^{13}C–KIEs are quite high compared to the measured KIEs, and (ii) the generation of $[Re^{I}(bpy)(CO)_3]^-$ is not very likely in photocatalytic CO_2 reduction by **1** in the presence of TEOA as the sacrificial electron donor.

Table 1. Computed ^{13}C–KIEs and their contributions at the M06 level of theory in ACN

TS	^{13}C KIE	$^{13}\nu_{RC}$	ZPE	MMI	EXC
[(bpy)$Re^{0\cdots}CO_2$] (TS-I)	1.061	1.011	1.053	1.020	0.978
[(bpy)$Re^{-I\cdots}CO_2$]$^-$ (TS-II)	1.086	1.033	1.071	0.995	0.986
[$Re^{I}C(O)OH^{\cdots}TEOAH^+$]$^+$ (TS-III)	1.048	1.018	1.049	0.983	0.999
[$Re^{0}C(O)OH^{\cdots}TEOAH^+$] (TS-IV)	1.048	1.018	1.050	0.984	0.997

Recently, Ishitani and co-workers demonstrated that the [Re^{I}(bpy)$(CO)_3$(TEOA-H^+)] adduct could form in DMF, and CO_2 can be captured by these complexes to generate a carbonate species which is proposed to be the active form of the catalyst in the photoreduction of CO_2. To confirm these results, we performed DFT calculations on the feasibility of the Re-carbonate species to act as the key intermediate of the photochemical CO_2 reduction cycle. Assuming the DMF adduct, [Re(bpy)$(CO)_3$(DMF)]$^+$, as the starting material, displacement of the solvent molecule by TEOA is thermodynamically downhill (−1.2 kcal/mol, Scheme 2); however, the subsequent combined deprotonation and CO_2 binding steps to form the carbonate species is only slightly uphill (7.4 kcal/mol) and could be enhanced in the presence of bases with higher pK_a than TEOA. Next, we calculated the associated potentials to reduce the Re-carbonate complexes. The computations indicate that the Re-DMF complex, [Re^{I}(bpy)$(CO)_3$(DMF)]$^+$, has first and second reduction potentials of −1.87 V and −2.00 V vs SCE, respectively. More negative

potentials are predicted for the first (−2.11 V vs SCE) and second (−2.78 V vs SCE) reduction of the Re-carbonate species. One assumption for these computed reduction potentials is that the ligands remain bound to the Re center (*see below for further discussion*). Analysis of the HOMO of the reduced $[Re^{I}(bpy)(CO)_3(DMF)]^-$ complex indicates that its reduction results in the formation of a $[Re^0\text{-}bpy^{\bullet-}]^-$-like intermediate, whereas reduction of the carbonate complex results in a species which resembles a doubly-reduced ligand, *i.e.*, a $[Re^{I}\text{-}bpy^{2-}]^-$-like species (Scheme S3). One likely scenario consistent with the ^{13}C−KIEs is the dissociation of the carbonate ligand upon the first reduction, which would generate $[Re^0(bpy)(CO)_3]$ so that similar active intermediates will be formed in both ACN and DMF solutions.

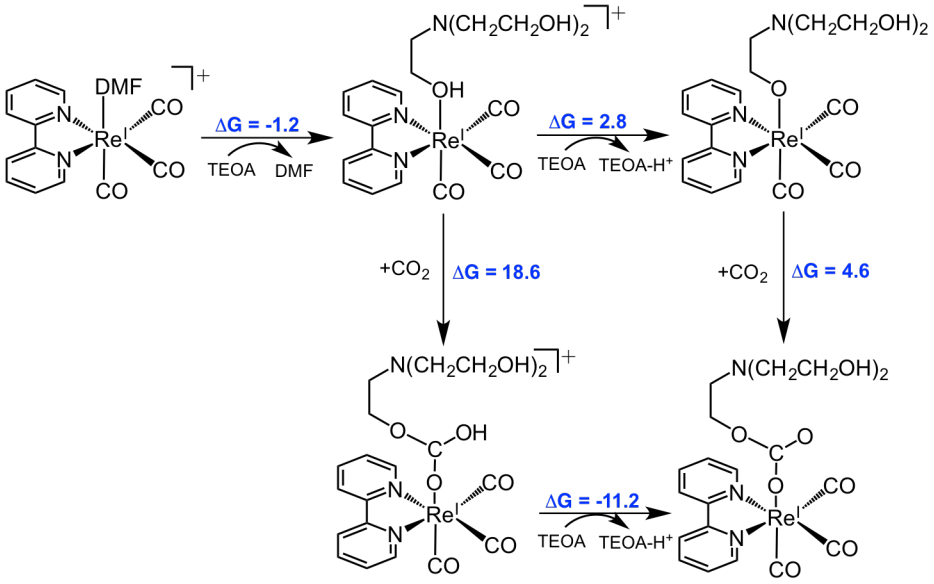

Scheme 2. Free energy changes in units of kcal/mol during the formation of the Re-carbonate species.

Finally, we investigated the formation of binuclear carboxylate species starting with $[Re^0(bpy)(CO)_3(CO_2)]$ and $[Re^0(bpy)(CO)_3]$ and found it to be favorable by 23.4 kcal/mol. In

principle, formation of such a species could lead to similar observed ^{13}C–KIEs because the binding of CO_2 to $[Re^0(bpy)(CO)_3]$ would necessarily be the first irreversible step. However, the formation of the binuclear species is shown to occur starting with photocleavage of a Re-Re dimer species in dry DMF and is not likely under the current experimental conditions.

DISCUSSION

Interpretation of ^{13}C Kinetic Isotope Effects. When only one step is isotopically sensitive, a competitive KIE permits the direct investigation of a transition state. For CO_2 reduction, however, more than one step is presumed to be isotopically sensitive. Thus, both CO_2 binding to the rhenium center and C-OH bond cleavage are expected to be contributors to the isotope effects given the changes in covalent bonding involved in these steps. Electron transfer reactions, such as the one depicted in eq. 3, can also be isotopically sensitive.[55,56] Protonation or deprotonation of a carboxylic acid can proceed with a small ^{13}C isotope effect,[57] especially in a proton transfer step to a species like $[Re^I(CO_2)(bpy)(CO)_3]^-$ which features a very low activation barrier. Although the equilibrium reaction between gaseous CO_2 and carbonate or bicarbonate in solution fractionates carbon in the system (1.0077 and 1.013 for bicarbonate and carbonate, respectively),[58] a contribution to the measured KIE from the formation of the monoalkyl carbonate derivative of TEOA is not expected because the R_0 value was determined from solutions of CO_2 in a mixture of solvent and TEOA in the presence of the catalyst without irradiation and in the absence of the catalyst. Therefore, any enrichment originating from the aforementioned equilibria is already taken into account in the measured KIE values.

Formulations for mechanisms with multiple isotopically sensitive steps have been proposed in the literature.[59] The advantage of using these formulations is that they allow a physical interpretation of the contributions from the intrinsic isotope effects. In eq. 14, it is

assumed that in the reaction catalyzed by **1**, CO_2 binding (eq. 2), the reduction producing $[Re^{I}(CO_2)(bpy)(CO)_3]^-$ (eq. 3), and the protonation followed by C-OH bond cleavage (eq. 4) are isotopically sensitive. The sensitivity to isotopic composition is obvious for eqs. 2 and 4, whereas the electron transfer (ET) reaction in eq. 3 is not straightforward. In ET reactions, KIEs originate from the changes in the classical nuclear barrier and the width of the nuclear tunneling barrier.[55] One example is that of Guarr *et al*. who reported ^{18}O–KIE values ranging from 1.04 to 1.09 for outer sphere redox reactions of hexaaquo Fe^{II}.[55] These data indicate that an ET reaction can have heavy atom isotope effects as large as 1.015.

$$^{13}C\ KIE = \frac{^{13}k_4 \times {}^{13}K_3 \times {}^{13}K_2 + \ {}^{13}k_3 \times {}^{13}K_2 \times \left(\frac{k_4}{k_{-3}}\right) + \ {}^{13}k_2 \times \left(\frac{k_4}{k_{-3}}\right) \times \left(\frac{k_3}{k_{-2}}\right)}{1 + \frac{k_4}{k_{-3}}\left(1 + \frac{k_3}{k_{-2}}\right)} \qquad (14)$$

The rate of ET, k_3, is expected to be faster than the rate of dissociation of CO_2 from the rhenium complex, k_{-2}. For example, the quenching of the ^{3}MLCT state of **1** by TEOA is 8.0×10^7 M^{-1} s^{-1} in degassed acetonitrile,[35] whereas loss of a ligand in the one-electron-reduced species, $[Re(bpy)(CO)_3Cl]^-$, is a slow process.[24] Although the triplet ligand field, ^{3}LF, excited states of rhenium diimine tricarbonyl complexes with phosphine ligands are thermally accessible from the triplet metal-to-ligand charge transfer state, ^{3}MLCT, this is not true for other ligands.[60] Taking these rate constants into account and assuming $k_3 >> k_{-2}$, eq. 14 can be reduced to eq. 15.

$$^{13}C\ KIE = \frac{^{13}k_4 \times {}^{13}K_3 \times {}^{13}K_2}{\left(\frac{k_4}{k_{-3}}\right)\left(\frac{k_3}{k_{-2}}\right)} + \ {}^{13}k_2 \qquad (15)$$

Studies of quenching with TEOA have shown that the oxidized $TEOA^{\bullet+}$ rapidly deprotonates from its α-carbon to produce an α-amino radical which has the ability to reduce rhenium (I) complexes.[35] Therefore, the decomposition of the oxidized TEOA makes the quenching step irreversible.[35] We can assume that $k_4/k_{-3} > 100$, indicating that C-OH bond cleavage is at least 100-fold more likely to occur than the back ET from the $[Re^{I}(CO_2)(bpy)(CO)_3]^-$ species. The DFT calculations presented herein indicate that the product of $^{13}k_4$ and $^{13}K_2$ is 1.097. Since it can be safely assumed that EIEs for the ET process range from 1.01 to 1.02,[55,56,61] the numerator in eq. 15, $^{13}k_4 \times {}^{13}K_3 \times {}^{13}K_2$, ranges from 1.11-1.12. Overall, the contribution of the first term in eq. 15 to the observed ^{13}C–KIE can only be as large as 0.01. Given that our calculated $^{13}k_2$ is 1.061, the overall ^{13}C–KIE could range from 1.06 to 1.07. This range is in good agreement with the measured values for the CO_2 reduction reactions in both ACN and DMF. The fact that we measured a similar ^{13}C–KIE for the reaction performed in ACN in the presence of $Ru(bpy)_3^{2+}$ validates our assumption that $k_3 >> k_{-2}$.

$$^{13}\text{C } KIE = \frac{^{13}k_4 \times {}^{13}K_6 + {}^{13}k_6 \times \left(\frac{k_4}{k_{-6}}\right)}{1 + \frac{k_4}{k_{-6}}} \qquad (16)$$

Alternatively, if a second reduction occurs before CO_2 binding as shown in eqs. 5-6, followed by eq. 4, the expression shown in eq. 16 describes the observed KIE on the reduction of CO_2. Although the formation of $[Re^{-I}(bpy)(CO)_3]^-$ has been shown to be unlikely under these conditions, the analysis of this possibility offers further insight.[35] For this, we must first estimate the ratio of the intrinsic rate constants k_4 and k_{-6}. Unfortunately, to the best of our knowledge, these intrinsic rate constants have not been determined. We can, however, solve for three different cases: (1) $k_4 >> k_{-6}$, (2) $k_4 << k_{-6}$, and (3) $k_4 \approx k_{-6}$. In the first case, eq. 16 is reduced to

^{13}C–KIE = $^{13}k_6$. Based on our DFT-calculated $^{13}k_6$, ^{13}C–KIE = 1.0862. This value is considerably larger than the experimental KIE. In the second case, the KIE must be equal to or larger than the product $^{13}k_4 \times {}^{13}K_6$, 1.097 based on our computations, a value that is also larger than the measured KIE. Finally, if $k_4 \approx k_{-6}$, the observed KIE value will approximate to 1.091, which does not compare well with the experimental measurements either. Therefore, on the basis of the measured ^{13}C–KIEs, $[Re^{I}(bpy)(CO)_3]^-$ is less likely than $[Re^{0}(bpy)(CO)_3]$ to be the nucleophile in the photochemical reduction of CO_2 by **1** when TEOA is the electron donor.

Physical Origins of ^{13}C Kinetic Isotope Effects. The calculated KIEs can be further analyzed to provide insights into the contributions to the isotopic discrimination by the various terms, namely $^{13}\nu_{RC}$ and $^{13}K_{TS}$ ($^{13}K_{TS}$= ZPE×EXC×VP). The DFT calculations in this study indicate that for both the CO_2-binding and C-OH bond cleavage steps $^{13}K_{TS}$ is the main contributor to the large intrinsic KIEs (Table 1). A dominant ZPE term is responsible for the large $^{13}K_{TS}$ values. The $^{13}\nu_{RC}$ values, which are defined as the ratio of light to heavy imaginary frequencies, are also larger than 1.0. The difference observed in the intrinsic KIEs between the **TS-I** and **TS-II** are due to the $^{13}\nu_{RC}$ contributions, with that of **TS-II** being three times as large as that of **TS-I**. Interestingly, the $^{13}\nu_{RC}$ values are not affected by the difference in the oxidation state of the rhenium center in **TS-III** and **TS-IV**. For comparison, in the case of O-O bond formation for water oxidation by ferrate, the analysis of the calculated KIEs concluded that its normal nature is a consequence of $^{18}\nu_{RC}$.[43]

CONCLUSIONS

In summary, our data show large and normal ^{13}C kinetic isotope effects during the photocatalytic reduction of CO_2 in acetonitrile or dimethylformamide using **1** as a catalyst and TEOA as the sacrificial electron donor. The similarity between the measured ^{13}C–KIEs in both

solvents (~1.07) suggests that the reactions involve the same first irreversible step, although with subtle variations in their transition state structures. Additionally, we calculated the KIEs and EIEs associated with the different steps in the reaction using DFT calculations and demonstrated excellent agreement between experimental and computed values. Analysis of the data combined with the computational studies indicates that the measured ^{13}C–KIEs are dominated by the intrinsic KIE of the first irreversible step, CO_2 binding. The latter is a novel observation that allows experimental access to the nature of the transition state during CO_2-binding by means of DFT calculations. The kinetic analysis allowed us to determine that the [Re^0(bpy)$(CO)_3$] species, is the nucleophile under photocatalytic conditions. After CO_2 binding, the following steps have low activation energies up to the C–OH bond cleavage step. Although the intrinsic ^{13}C–KIE for C-OH bond heterolysis is large, 1.048, its contribution to the overall ^{13}C KIE amounts to ≤ 1 %. This report serves as a reference point for mechanisms associated with CO_2 activation and highlights the fact that a combined natural abundance competitive KIE measurements and DFT calculations approach is a powerful and useful methodology to probe mechanistic aspects of CO_2 reduction.

EXPERIMENTAL SECTION

Materials. 2,2□–bipyridine (bpy), pentacarbonylchlororhenium (I), and triethanolamine (TEOA) were all purchased from Sigma-Aldrich and used as received. Ruthenium (III) chloride trihydrate was purchased from Pressure Chemical Company and used as received. Re(bpy)$(CO)_3$Cl and [Ru$(bpy)_3$]Cl_2 were both synthesized according to the literature. Solvents used in this work were purified by passing through a solvent purification system (Glass Contour). ^{1}H and ^{13}C NMR spectra were recorded on a Bruker AVANCE (300 MHz) or Bruker AVANCE III (400 MHz)

system at ambient temperature and were referenced to residual solvent peaks. UV-Vis spectra were recorded on a Cary 50 spectrophotometer.

Synthesis. $Re(bpy)(CO)_3Cl$ was prepared with slight modifications from previously reported methods.[62] Three different batches were prepared for the current experiments. Briefly, in a 100 mL round bottom flask, $Re(CO)_5Cl$ (0.502g, 1.35 mmol), 2,2□-bipyridine (0.211g, 1.35 mmol) and toluene (50 mL) were added together and the resultant reaction mixture was heated under refluxing conditions for 5 hours. Upon cooling, the product was vacuum filtered, and rinsed with cold toluene. ^1H NMR (δ, 400 MHz, DMSO-d_6): 9.02 (d, 1H), 8.77 (d, 1H), 8.34(t, 1H), 7.76(t, 1H). FT-IR (acetonitrile): 2022 (vs), 1917 (s), 1900 (s). Anal. Found for $C_{13}H_8N_2O_3ClRe$: C, 40.30; H, 2.05; N, 5.76. Calcd. C, 40.47: H, 1.75; N, 6.06.

KIE determination. The reaction and collection of samples was done using the apparatus shown in Figure 3. To the graduated solvent reservoir was added a solution that was five parts solvent to one part TEOA, where the solvent was either acetonitrile or dimethylformamide. The undissolved catalyst was pre-weighed in such a way that its concentration would 2 mM, 1 mM, or 0.5 mM once dissolved in solution, depending on individual reactions, and added to the lower bulb of the reaction vessel. From the right of valve 1, onwards, the manifold was evacuated down to approximately 0.2 torr. Valves 3 and 4 were then closed. After saturating the solvent/TEOA mixture with a gas mixture that was 3% CO_2 in N_2, a 20.0 ml portion was introduced into the lower bulb of the reaction vessel by opening valve 1. The lower bulb has a volume of 30.0 ml, so the headspace above the solution was 10.0 mL. The vessel was then removed from the manifold setup, and positioned in front of an ORIEL lamp with a 1000V FEL bulb, and a 350-450 nm band pass filter. For experiments that included the catalyst but not the photosensitizer, reaction times ran from 16 to 72 hours to obtain a range of

CO_2 conversion fractions. When the photosensitizer was used, the reaction time dropped dramatically. Run times of only 30 to 60 minutes were required to achieve the same amounts of CO_2 conversion. Once these reactions were performed, the reaction vessel was re-attached to the KIE manifold.

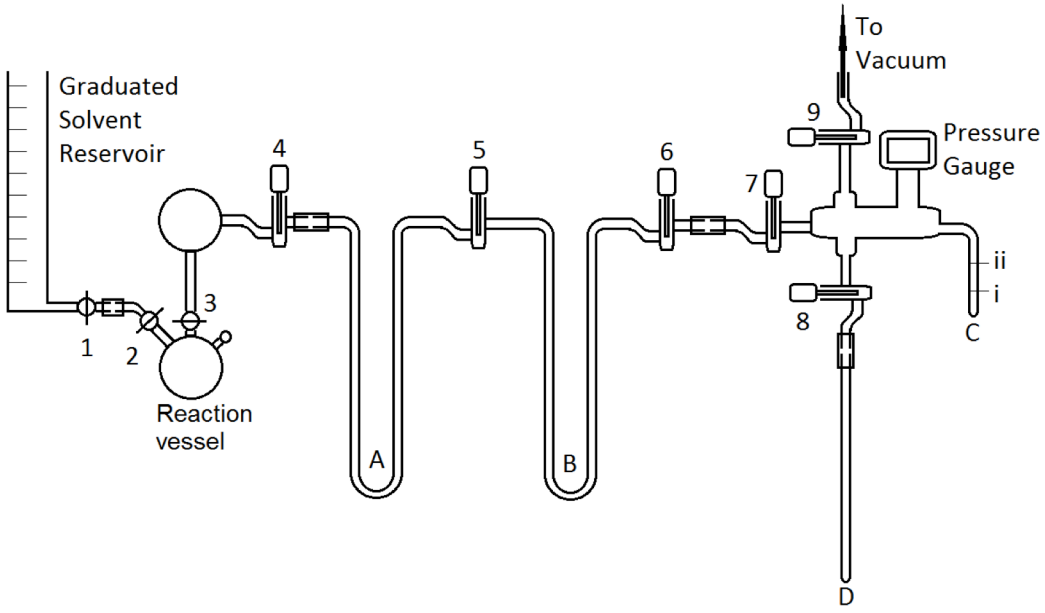

Figure 3. Vacuum apparatus for the determination of ^{13}C isotope effects.

The remaining unreacted CO_2 was then collected as follows. Solvent trap A was immersed in a bath of liquid nitrogen. Valve 5 was closed, and valves 4 and 3 were opened, in that order. The reaction mixture would start to bubble as the sudden vacuum would cause it to outgas. A mixture of gases and the respective solvent were collected in trap A. Valve 3 was closed after 2.5 minutes of constant outgassing from the reaction mixture. Valve 4 was left open for an additional five minutes. Valve 4 was then closed, and the liquid nitrogen was removed from trap A. The frozen solvent was given time to melt and collect at the bottom of trap A. Trap B was then immersed in liquid nitrogen, and valve 6 was closed. Trap A was then immersed in a cold bath of isopropanol/dry ice. This kept the solvent frozen, but allowed the gas to transfer

over into trap B. Valve 5 was opened for ten minutes. Valves 4 and 6 were then also opened, to evacuate the N_2 and CO. The liquid nitrogen is cold enough that it keeps the CO_2 frozen, even at such low pressures. The same is true for the ability of the isopropanol/dry ice bath to retain the frozen solvent. Once the pressure of the system had dropped back down to 0.2 torr, valves 5 and 6 were closed. The liquid nitrogen bath over trap B was replaced with the isopropanol/dry ice bath. The bottom one-third of trap C was immersed in liquid nitrogen (approximately at marking *i*). Valves 8 and 9 were closed, and then valve 6 was opened. The pressure initially increased, but quickly declined as the CO_2 condensed in trap C. After ten minutes the pressure would have leveled off. The level of liquid nitrogen was then increased so that at least two-thirds of trap C was immersed (approximately marking *ii*). Valve 7 was closed. Valve 9 was opened to evacuate any uncondensed gasses, such as N_2 or CO. The liquid nitrogen is cold enough that the CO_2 in trap C will not evaporate, even at these low pressures. Valve 9 was closed, and the pressure was recorded as P_{low}. The liquid nitrogen was removed from trap C, and the pressure increased as the CO_2 sublimated. After a few minutes, the pressure leveled off, and this was recorded as P_{high}. The difference between P_{high} and P_{low} should be P_{CO2} (Note: The CO_2 pressure measured when no reaction occurs should be measured experimentally and recorded as a blank ($P°$)). After P_{CO2} had been measured, the removable tube, labeled as trap D, was immersed in liquid nitrogen, and valve 8 was opened. Once all CO_2 had been collected, the liquid nitrogen level was raised slightly, and valve 9 was opened briefly. Valve 8 was then closed, and a torch was used to seal the tube 10 cm up from the bottom. The liquid nitrogen was removed, and the torch was used to completely remove the 10 cm segment from the rest of the apparatus.

The enrichment of the residual carbon dioxide was analyzed by isotope ratio mass spectrometry (IRMS) using a dual-inlet instrument. The unreacted CO_2 was isolated and purified

as described above. The calculated turnover number (TON) in the reactions ranged from 0.3 to 7.1. The TON was calculated from the ratio of moles of reacted CO_2 to moles of catalyst used. As previously observed by Hawecker *et al*., control reactions in the absence of **1** did not result in the consumption of CO_2.[29]

Computational Methods. All geometries were fully optimized at the M06 level of density functional theory[63] with the SMD aqueous continuum solvation model[64] using the Stuttgart [8s7p6d2f | 6s5p3d2f] ECP60MWB contracted pseudopotential basis set[65] on Re and the 6-31G(d) basis set on all other atoms.[66] Non-analytical integrals were evaluated using the integral=grid=ultrafine option as implemented in the Gaussian 09 software package.[67] The nature of all stationary points was verified by analytic computation of vibrational frequencies, which were also used for the computation of zero-point vibrational energies, molecular partition functions (with all frequencies below 50 cm^{-1}, with the exception of the imaginary frequency of transition states, replaced by 50 cm^{-1} when computing free energies), and for determining the reactants and products associated with each transition-state structure (by following the normal modes associated with imaginary frequencies). Partition functions were used in the computation of 298 K thermal contributions to the free energy employing the usual ideal-gas, rigid-rotator, harmonic oscillator approximation.[68] Free-energy contributions were added to single-point, SMD-solvated M06 electronic energies computed at the optimized geometries obtained with the initial basis with the SDD basis set on Re and the larger 6-311+G(2df,p) basis set on all other atoms to arrive at final, composite free energies. The quenching studies with TEOA have shown that the oxidized $TEOA^{\bullet+}$ rapidly deprotonates from its α-carbon to produce an α-amino radical[35] and TEOA itself could be the proton acceptor to generate $TEOAH^+$, which is employed as the proton donor species in the current work for modeling of the CO_2 reduction mechanism. As an

additional note, throughout the manuscript and supporting information, the formal oxidation state of Re has been depicted for the sake of clarity even though in some cases the electronic structure of the complexes is more complicated and assignment of oxidation states is not straightforward.

ASSOCIATED CONTENT

Supporting Information. Computational details and complete calculated vibrational frequencies. This material is available free of charge via the Internet at http://pubs.acs.org.

AUTHOR INFORMATION

Corresponding Author

*E-mail for M.Z.E: mzertem@bnl.gov

*E-mail for A.M.A.-B: alfredo.angeles-boza@uconn.edu.

Author Contributions

The manuscript was written through contributions of all authors. All authors have given approval to the final version of the manuscript.

Notes

The authors declare no competing financial interest.

ACKNOWLEDGMENT

A.M.A.-B. thanks the University of Connecticut for start-up funds. The work carried out at Brookhaven National Laboratory (M.Z.E. and J.T.M.) was supported by the U.S. Department of Energy, Office of Science, Division of Chemical Sciences, Geosciences, & Biosciences, Office

of Basic Energy Sciences under contract DE-SC00112704. The authors would also like to thank Dr. Etsuko Fujita for discussions and advice.

REFERENCES

(1) Appel, A. M.; Bercaw, J. E.; Bocarsly, A. B.; Dobbek, H.; DuBois, D. L.; Dupuis, M.; Ferry, J. G.; Fujita, E.; Hille, R.; Kenis, P. J. A.; Kerfeld, C. A.; Morris, R. H.; Peden, C. H. F.; Portis, A. R.; Ragsdale, S. W.; Rauchfuss, T. B.; Reek, J. N. H.; Seefeldt, L. C.; Thauer, R. K.; Waldrop, G. L. *Chem. Rev*. **2013,** *113,* 6621-6658.

(2) Liu, C.; Dubois, K. D.; Louis, M. E.; Vorushilov, A. S.; Li, G. *ACS Catal.* **2013,** *3,* 655-662.

(3) Agarwal, J.; Shaw, T. W.; Stanton, C. J.; Majetich, G. F.; Bocarsly, A. B.; Schaefer, H. F. *Angew. Chem. Int. Ed.* **2014,** *53,* 5152-5155.

(4) Sampson, M. D.; Nguyen, A. D.; Grice, K. A.; Moore, C. E.; Rheingold, A. L.; Kubiak, C. P. *J. Am. Chem. Soc.* **2014,** *136,* 5460-5471.

(5) White, T. A.; Maji, S.; Ott, S. *Dalton Trans.* **2014,** *43,* 15028-15037.

(6) Roldan, A.; Hollingsworth, N.; Roffey, A.; Islam, H. U.; Goodall, J. B. M.; Catlow, C. R. A.; Darr, J. A.; Bras, W.; Sankar, G.; Holt, K. B.; Hogarth, G.; de Leeuw, N. H. *Chem. Commun.* **2015,** *51,* 7501-7504.

(7) Medina-Ramos, J.; DiMeglio, J. L.; Rosenthal, J. *J. Am. Chem. Soc*. **2014,** *136,* 8361-8367.

(8) Takeda, H.; Koizumi, H.; Okamoto, K.; Ishitani, O. *Chem. Commun.* **2014,** *50,* 1491-1493.

(9) Chan, S. L.-F.; Lam, T. L.; Yang, C.; Yan, S.-C.; Cheng, N. M. *Chem. Commun.* **2015,** *51,* 7799-7801.

(10) Fei, H.; Sampson, M. D.; Lee, Y.; Kubiak, C. P.; Cohen, S. M. *Inorg. Chem.* **2015,** *54,* 6821-6828.

(11) Manbeck, G. F.; Muckerman, J. T.; Szalda, D. J.; Himeda, Y.; Fujita, E. *J. Phys. Chem. B* **2015,** *119,* 7457-7466.

(12) Matlachowski, C.; Braun, B.; Tschierlei, S.; Schwalbe, M. *Inorg. Chem.* **2015,** *54,* 10351-10360.

(13) Mohamed, E. A.; Zahran, Z. N.; Naruta, Y. *Chem. Commun.* **2015,** *51,* 16900-16903.

(14) Therrien, J. A.; Wolf, M. O.; Patrick, B. O. *Inorg. Chem.* **2015,** *54,* 11721-11732.

(15) Kuriki, R.; Ishitani, O.; Maeda, K. *ACS Appl. Mater. Interfaces* **2016,** *8*, 6011-6018.

(16) Neri, G.; Aldous, I. M.; Walsh, J. J.; Hardwick, L. J.; Cowan, A. J. *Chem. Sci.* **2016,** *7,* 1521-1526.

(17) Schreier, M.; Luo, J.; Gao, P.; Moehl, T.; Mayer, M. T.; Gratzel, M. *J. Am. Chem. Soc.* **2016,** *138,* 1938-1946.

(18) Huckaba, A. J.; Sharpe, E. A.; Delcamp, J. H. *Inorg. Chem.* **2016,** *55,* 682-690.

(19) Morimoto, T.; Nakajima, T.; Sawa, S.; Nakanishi, R.; Imori, D.; Ishitani, O. *J. Am. Chem. Soc.* **2013,** *135,* 16825-16828.

(20) Kou, Y.; Nabetani, Y.; Masui, D.; Shimada, T.; Takagi, S.; Tachibana, H.; Inoue, H. *J. Am. Chem. Soc.* **2014,** *136,* 6021-6030.

(21) Machan, C. W.; Sampson, M. D.; Chabolla, S. A.; Dang, T.; Kubiak, C. P. *Organometallics* **2014,** *33*, 4550-4559.

(22) Riplinger, C.; Sampson, M. D.; Ritzmann, A. M.; Kubiak, C. P.; Carter, E. A. *J. Am. Chem. Soc.* **2014,** *136,* 16285-16298.

(23) Riplinger, C.; Carter, E. A. *ACS Catal.* **2015,** *5,* 900-908.

(24) Sullivan, B. P.; Bolinger, C. M.; Conrad, D.; Vining, W. J.; Meyer, T. J. *J. Chem. Soc., Chem. Commun.* **1985,** *20,* 1414-1416.

(25) Hawecker, J.; Lehn, J. M.; Ziessel, R. *Helv. Chim. Acta* **1986,** *69,* 1990-2012.

(26) Fujita, E.; Muckerman, J. T. *Inorg. Chem.* **2004,** *43,* 7636-7647.

(27) Sampson, M. D.; Froehlich, J. D.; Smieja, J. M.; Benson, E. E.; Sharp, I. D.; Kubiak, C. P. *Energy Environ. Sci.* **2013,** *6,* 3748-3755.

(28) Hori, H.; Johnson, F. P. A.; Koike, K.; Ishitani, O.; Ibusuki, T. *J. Photochem. Photobiol., A* **1996,** *96,* 171-174.

(29) Hawecker, J.; Lehn, J.-M.; Ziessel, R. *J. Chem. Soc., Chem. Commun.* **1983,** *9,* 536-538.

(30) Grice, K. A.; Gu, N. X.; Sampson, M. D.; Kubiak, C. P. *Dalton Trans.* **2013,** *42,* 8498-8503.

(31) Benson, E. E.; Sampson, M. D.; Grice, K. A.; Smieja, J. M.; Froehlich, J. D.; Friebel, D.; Keith, J. A.; Carter, E. A.; Nilsson, A.; Kubiak, C. P. *Angew. Chem., Int. Ed.* **2013,** *52,* 4841-4844.

(32) Takeda, H.; Koike, K.; Inoue, H.; Ishitani, O. *J. Am. Chem. Soc.* **2008,** *130,* 2023-2031.

(33) Kutal, C.; Weber, M. A.; Ferraudi, G.; Geiger, D. *Organometallics* **1985,** *4,* 2161-2166.

(34) Kutal, C.; Corbin, A. J.; Ferraudi, G. *Organometallics* **1987,** *6,* 553-557.

(35) Kalyanasundaram, K. *J. Chem. Soc., Faraday Trans. 2* **1986,** *82,* 2401-2415.

(36) Hori, H.; Johnson, F. P. A.; Koike, K.; Takeuchi, K.; Ibusuki, T.; Ishitani, O. *J. Chem. Soc., Dalton Trans.* **1997,** *6, 1019-1024.*

(37) Hayashi, Y.; Kita, S.; Brunschwig, B. S.; Fujita, E. *J. Am. Chem. Soc.* **2003,** *125,* 11976-11987.

(38) Morris, A. J.; Meyer, G. J.; Fujita, E. *Acc. Chem. Res.* **2009,** *42,* 1983-1994.

(39) Agarwal, J.; Fujita, E.; Schaefer, H. F.; Muckerman, J. T. *J. Am. Chem. Soc.* **2012,** *134,* 5180-5186.

(40) Christensen, N. J.; Fristrup, P. *Synlett* **2015,** *26,* 508-513.

(41) Klinman, J. P. *The FEBS journal* **2014,** *281,* 489-497.

(42) Angeles-Boza, A. M.; Roth, J. P. *Inorg. Chem.* **2012,** *51,* 4722-4729.

(43) Sarma, R.; Angeles-Boza, A. M.; Brinkley, D. W.; Roth, J. P. *J. Am. Chem. Soc.* **2012,** *134,* 15371-15386.

(44) Angeles-Boza, A. M.; Ertem, M. Z.; Sarma, R.; Ibanez, C. H.; Maji, S.; Llobet, A.; Cramer, C. J.; Roth, J. P. *Chem. Sci.* **2014,** *5,* 1141-1152.

(45) Khan, S.; Yang, K. R.; Ertem, M. Z.; Batista, V. S.; Brudvig, G. W. *ACS Catal.* **2015,** *5,* 7104-7113.

(46) Cleland, W. W. *Arch. Biochem. Biophys*. **2005,** *433,* 2-12.

(47) Ruszczycky, M. W.; Anderson, V. E. *J. Theor. Biol.* **2006,** *243,* 328-342.

(48) Schneider, T. W.; Angeles-Boza, A. M. *Dalton Trans.* **2015,** *44,* 8784-8787.

(49) Young, R. C.; Keene, F. R.; Meyer, T. J. *J. Am. Chem. Soc.* **1977,** *99,* 2468-2473.

(50) Gholamkhass, B.; Mametsuka, H.; Koike, K.; Tanabe, T.; Furue, M.; Ishitani, O. *Inorg. Chem.* **2005,** *44,* 2326-2336.

(51) Tian, G.; Berry, J. A.; Klinman, J. P. *Biochemistry* **1994,** *33,* 226-234.

(52) Smieja, J. M.; Benson, E. E.; Kumar, B.; Grice, K. A.; Seu, C. S.; Miller, A. J. M.; Mayer, J. M.; Kubiak, C. P. *Proc. Natl. Acad. Sci. U. S. A.* **2012,** *109,* 15646-15650.

(53) Bigeleisen, J.; Mayer, M. G. *J. Chem. Phys.* **1947,** *15,* 261-267.

(54) Jacob, B. In *Isotope Effects In Chemistry and Biology*; CRC Press: 2005, p 1.

(55) Guarr, T.; Buhks, E.; McLendon, G. *J. Am. Chem. Soc.* **1983,** *105,* 3763-3767.

(56) Guarr, T.; McLendon, G. *Coord. Chem. Rev.* **1985,** *68,* 1-52.

(57) Bayles, J. W.; Bron, J.; Paul, S. O. *J. Chem. Soc., Farad. Trans. 1* **1976,** *72,* 1546-1552.

(58) Thode, H. G.; Shima, M.; Rees, C. E.; Krishnamurty, K. V. *Can. J. Chem.* **1965,** *43,* 582-595.

(59) Cook, P. F.; Cleland, W. W. *Enzyme Kinetics and Mechanism*; 1 ed.; Garland Science: New York, 2007.

(60) Koike, K.; Okoshi, N.; Hori, H.; Takeuchi, K.; Ishitani, O.; Tsubaki, H.; Clark, I. P.; George, M. W.; Johnson, F. P. A.; Turner, J. J. *J. Am. Chem. Soc.* **2002,** *124,* 11448-11455.

(61) Diebler, H.; Dodel, P. H.; Taube, H. *Inorg. Chem.* **1966,** *5,* 1688-1691.

(62) Smieja, J. M.; Kubiak, C. P. *Inorg. Chem.* **2010,** *49,* 9283-9289.

(63) Zhao, Y.; Truhlar, D. G. *Theor. Chem. Acc.* **2008,** *120,* 215-241.

(64) Marenich, A. V.; Cramer, C. J.; Truhlar, D. G. *J. Phys. Chem. B* **2009,** *113,* 6378-6396.

(65) Andrae, D.; Häussermann, U.; Dolg, M.; Stoll, H.; Preuß, H. *Theor. Chim. Acta,* **1990,** *77,* 123-141.

(66) Hehre, W. J. AB INITIO *Molecular Orbital Theory*; Wiley, 1986.

(67) Frisch, M. J.; Trucks, G. W.; Schlegel, H. B.; Scuseria, G. E.; Robb, M. A.; Cheeseman, J. R.; Scalmani, G.; Barone, V.; Mennucci, B.; Petersson, G. A.; Nakatsuji, H.; Caricato, M.; Li, X.; Hratchian, H. P.; Izmaylov, A. F.; Bloino, J.; Zheng, G.; Sonnenberg, J. L.; Hada, M.; Ehara, M.; Toyota, K.; Fukuda, R.; Hasegawa, J.; Ishida, M.; Nakajima, T.; Honda, Y.; Kitao, O.; Nakai, H.; Vreven, T.; Montgomery Jr., J. A.; Peralta, J. E.; Ogliaro, F.; Bearpark, M. J.; Heyd, J.; Brothers, E. N.; Kudin, K. N.; Staroverov, V. N.; Kobayashi, R.; Normand, J.; Raghavachari, K.; Rendell, A. P.; Burant, J. C.; Iyengar, S. S.; Tomasi, J.; Cossi, M.; Rega, N.; Millam, N. J.; Klene, M.; Knox, J. E.; Cross, J. B.; Bakken, V.; Adamo, C.; Jaramillo, J.; Gomperts, R.; Stratmann, R. E.; Yazyev, O.; Austin, A. J.; Cammi, R.; Pomelli, C.; Ochterski, J. W.; Martin, R. L.; Morokuma, K.; Zakrzewski, V. G.; Voth, G. A.; Salvador, P.; Dannenberg, J. J.; Dapprich,

S.; Daniels, A. D.; Farkas, Ö.; Foresman, J. B.; Ortiz, J. V.; Cioslowski, J.; Fox, D. J.; Gaussian, Inc.: Wallingford, CT, USA, 2009.

(68) Cramer, C. J. *Essentials of Computational Chemistry: Theories and Models*; Wiley, 2013.

Insert Table of Contents Graphic Here

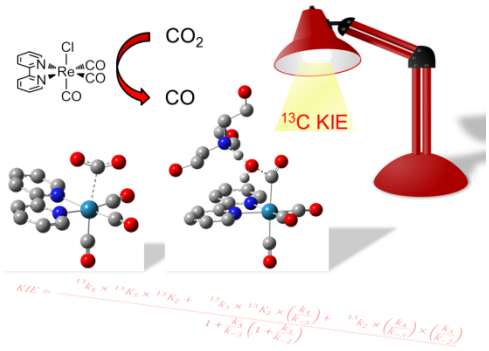
Cl
Re
CO
CO
CO
CO2
CO
13C KIE